Estimate of Large CZT Detector Absolute Efficiency

J. M. Pérez, *Member, IEEE*, Z. He, *Senior Member, IEEE*, D. K. Wehe, *Senior Member, IEEE*, and Y. F. Du

***Abstract*—This paper presents a simulation of the spectroscopic performance of two large CZT coplanar detectors, 1.5 × 1.5 cm^2 area and 1.0 cm thick, with coplanar anodes. A code, based on the GEANT libraries and classical Monte Carlo sampling, was developed to simulate experimental scenarios. This code adapts the GEANT capabilities for simulating complex detection systems for spectroscopic studies. Detectors with perfect charge transport and collection were first simulated. The code was benchmarked by simulating an HPGe detector. The result for this detector is used for estimating the code's capabilities. Results from the simulation of this basic detector model are presented and discussed. Subsequently, the effects of a possible realistic electric field profile in a coplanar detector unable to efficiently deflect electrons to the collecting anode is studied. From the analysis of the differences found between the simulated and measured results, some conclusions relating the electrode design and detector quality are proposed.**

***Index Terms*—CdZnTe, CZT, Monte Carlo methods, radiation detectors, simulation.**

I. Overview of This Paper

LARGER volume CdZnTe crystals are now available for manufacturing high-efficiency gamma radiation detectors. In spite of the improved quality of the material and device construction, the low mobility of holes, nearly one order of magnitude below the value for electrons, remains the main limitation to large-volume spectrometry with this material. This problem has been successfully overcome by methods that are insensitive to the hole drift. Among them, the use of coplanar grid anodes [1] has yielded noteworthy results for single detectors [2].

The spectroscopic performance of two CZT coplanar detectors having 1.5 × 1.5 cm^2 area and 1 cm thickness has been reported earlier [3]. These two units, known as I9-04 and I9-01, were produced by eV Products[1] using the electrode pattern described in [4] and schematically shown in Fig. 1. The two detectors showed slightly different energy resolutions: 2.0 and 2.3% for the 662-keV ^{137}Cs photopeak, respectively. A more careful inspection reveals interesting differences in the spectroscopic responses of these two detectors in the photopeak efficiency and the shape of the Compton edge at lower energies.

Manuscript received November 15, 2001; revised March 22, 2002. This work was supported in part by the U.S. Department of Energy under Grant DE-FG08-98NV13357 and by the Spanish Ministry of Education under Grant PR1999-0177 0076243636.

J. M. Pérez is with CIEMAT, Madrid E-28040, Spain (e-mail: jm.perez@ciemat.es).

Z. He and D. K. Wehe is with the Department of Nuclear Engineering and Radiological Sciences, The University of Michigan, Ann Arbor, MI 48109 USA (e-mail: dkw@umich.edu; hezhong@umich.edu).

Y. F. Du is with CT Lab, Global Imaging Technology Center, General Electric, Niskayuna, NY 12309 USA (e-mail: duy@cdr.ge.comu).

Digital Object Identifier 10.1109/TNS.2002.801512

[1]eV Products, Saxonburg, PA.

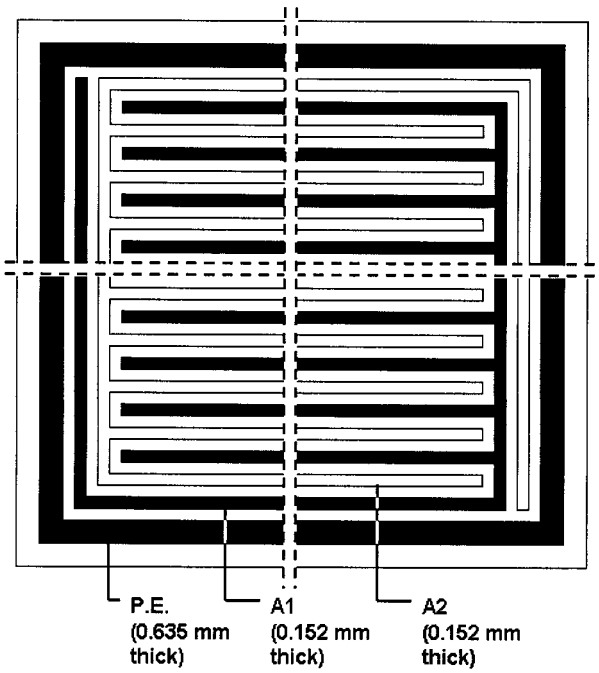

Fig. 1. Schematic viewgraph of the coplanar anode grid pattern of the CdZnTe detectors considered in this paper. The peripheral electrode (P.E.) acts as guard ring. Anodes 1 (A1) and 2 (A2) are composed by 13 horizontal strips and two vertical ones. Gap width is 0.355 mm.

Looking at pulse waveforms, detector I9-04 showed pulses with an unexpected residual positive contribution in the signal induced at the noncollecting anode [3]. The proportion of incoming photons that generated this kind of anomalous waveform for several energies in the range of interest (^{133}Ba, ^{137}Cs, and ^{60}Co sources) was estimated to be ∼10% of the total acquired. This result indicates processes internal to the detector that alter the expected charge drift and/or collection, thus affecting the spectroscopic performance.

Diagnosing the cause of this problem and others related to unexpected carrier transport inside the crystal is not a trivial task. One way to obtain information about why the detector spectroscopic performance deviates from the expected performance is to simulate the detector behavior and explore the impact of variations in assumed parameters. The comparison of the real and expected absolute measurements should offer interesting information relating total and photopeak detector efficiency. Total absolute counting-rate losses would indicate possible dead regions in the detector, whereas discrepancies in the photopeak area would indicate regions in which charge is not ideally transported or collected.

Thus, the aim of this work is to simulate the absolute spectroscopic response of CZT ideal detectors for energies above

50 keV. The simulation models a radioactive source, defined by its activity, shape, and isotope, irradiating a detector surrounded by electronic components and shielding materials. Initially, detectors with perfect charge transport were simulated. Fluctuations in the energy due to electronic noise were modeled assuming Gaussian distribution functions.

Our predictive code was benchmarked by simulating an HPGe detector. The accuracy of the simulation for this detector in a geometry similar to that used for the CZT measurements establishes the code's predictive capabilities. After this study, some preliminary considerations are presented in order to correctly define the true sensitive volume of the actual CZT coplanar detectors. Results from the simulation of the ideal CZT detectors are presented and compared to actual results. Finally, the effects of a possible realistic electrical field profile unable to efficiently deflect the electrons to the collecting anode are analyzed.

II. Description of the Simulation Program

The simulation package used in this work was Fortran-based and used the GEANT v.3.21 [5] Linux version libraries. A C++ version was subsequently written when GEANT v. 4 [6] became available. In this work, versions 4.2.0 and 4.3.1 of GEANT4 have been used, together with version 0.3 of the electromagnetic low-energy processes package (G4EMLOW0.3). A set of custom Monte Carlo routines adapt the GEANT code, designed for simulation in high-energy physics and accelerator experiments, to spectroscopic purposes.

Effects due to nonideal carrier transport within the detector, or electronic distortions produced by the front-end electronics, have not been explicitly included in these simulations. Thus, the charge produced by each event in the active region of the detector crystal is transformed into a fast induced charge pulse. The amplitude of this pulse is proportional to the total charge generated by the photon in the crystal. Ballistic deficit is not considered. Electronic noise in the complete chain has been included in the simulation by introducing a distortion in the pulse amplitude by assuming a Gaussian distribution, in which the parameter σ is known from the experimental detector full-width at half-maximum (FWHM) value at the corresponding energy.

In the case of a real coplanar device, the spectrum is mainly degraded by electron trapping and the asymmetry between weighting potentials of the two anode grids. Other effects such as hole contributions, leakage current on the anode surface, or electronic noise are minor effects for the quality detectors and the energy range of interest in this work (300–1500 keV). Corrections for electron trapping are handled by adjusting the relative gain in the subtraction circuit of the anode preamplifiers stage [7].

Due to the weighting potential asymmetry, energy resolution should be best for photons interacting near the cathode and gradually become poorer for interactions nearer to the anode surface [4]. See [2] for a graphical explanation of this effect. The shape of photopeaks in coplanar detectors is mainly due to the dependence of the energy resolution on the interaction depth. Thus, the shape of photopeaks in this kind of device can be modeled as the superposition of a set of Gaussian curves with different standard deviations. For the simulations, the distortion in the energy spectrum due to this effect has been assigned for each event using the following rule: the peak broadening is calculated from the standard resolution calibration equation for the deposited energy. But if the interaction depth is smaller than 0.3 cm from the anode, this value is doubled, and if less than 0.1 cm, the value is quadrupled. Using this basic model, the shapes of the predicted peaks are similar to the experimental peaks. While this is a relatively simple approach, we are primarily concerned about other major causes of distortions due to coplanar collection techniques on the spectrum profile.

III. Verification of the Simulation Tool

A. Detector Reference

Cryogenically cooled Ge detectors are among the most precise and reliable detectors for quantitative spectroscopic measurements, and their performance should be predictable through simulation. A Ge detector, Canberra GX2018, has been adopted as the standard to check our code capability. It is an extended-range closed-end cylindrical coaxial detector 46 mm long and 52.5 mm in diameter, with a core hole 31 mm long and 7 mm in diameter. Physical characteristics of the experimental setup and detector, as reported by the vendor for this particular detector, have been included in the simulation. The uncertainty in the source–detector surface positioning is estimated to be $\sim$0.05 cm.

B. Results for Higher Energies

Two radioactive point sources with emission lines over 500 keV have been studied: ^{137}Cs (activity: 336 664 Bq $\pm$4%) and ^{60}Co (activity: 107 275 Bq $\pm$3%). Spectra were acquired using the described Ge detector with a live time preset to 300 s. A background spectrum was also acquired to subtract the background contribution from the source spectra. One simulation was run for each of the above radioactive sources, and 2K-channel simulated spectra were generated. Electronic noise in the preamplifier and shaper was taken into account simply by assuming Gaussian fluctuations in the total deposited energy, with rms values on the order of that measured in the experimental setup.

Fig. 2 shows examples of real and simulated spectra obtained for ^{60}Co. The only significant differences that can be observed qualitatively are small unexpected accumulations on both sides of the 1333 photopeak in the real spectrum. This affects the counting rate in the Compton region between peaks, with this region showing a significantly higher error that others in the spectrum. Poorer counting statistics (100 times lower than that in the 23–1169 keV region), pulse pileup, and nonuniform electric field profiles in the crystal (not considered in the simulation) can explain this effect.

Table I compares real and simulated spectra at higher energies. Differences in detector counting efficiency in the most relevant regions of the spectrum are given. General agreement is found, although differences in the photopeak areas are larger than those for total efficiency. As commented above, a signifi-

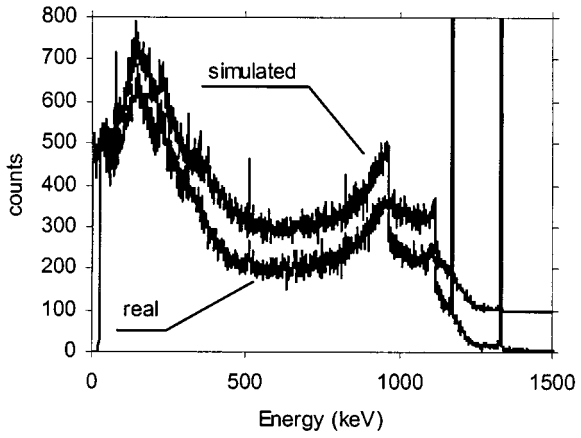

Fig. 2. Comparison of real (lower) and simulated (upper) spectra for the HPGe detector and the ^{60}Co source. Acquisition time corresponds to 300-s live time. Detector–source distance was 12.69 cm. The scale has been chosen in order to enhance the Compton edge profile. Simulated spectrum has been translated in the Y axis for a better comparison.

TABLE I
DIFFERENCES IN SIMULATED AND REAL HPGE DETECTOR EFFICIENCY AT HIGHER ENERGY

Isotope	Region	Energy	Efficiency Differences (Simulated - Measured)
137Cs	Compton	40 - 659 keV	0.9 %
	Photopeak	662 keV	3.8 %
	Total	40 - 1000 keV	0.8 %
	Peak (662 keV) to Total ratio:		3.2 %
60Co	Compton	23 - 1169 keV	2.7 %
	Photopeak	1173 keV	3.5 %
	Compton	1177 - 1328 keV	-20.1 %
	Photopeak	1333 keV	4.0 %
	Total	23 - 2000 keV	2.3 %
	Peak (1173 keV) to total ratio:		0.9 %
	Peak (1333 keV) to total ratio:		1.4 %

cant large error is found in the simulation of the Compton region between the two peaks (1177–1328 keV).

C. Results at Lower Energies

The study above was also extended to lower energies with the X-ray lines of the ^{137}Cs source and photopeaks of ^{133}Ba. Experimental and simulated results were acquired for a 230 734 Bq $\pm$4% ^{133}Ba point source in the geometry previously detailed. Quantitative differences between simulated and real photopeak areas and total detector counting efficiency are summarized in Table II.

An acceptable agreement is found in the total counting rate for the ^{133}Ba spectrum above 40 keV, but serious differences are found at lower energies. It can be seen from these results that lines under 40 keV are largely underestimated in the simulation, with larger differences for lower energies. Low-energy gamma peaks have an error larger than those obtained at higher energies, $\sim$10% in the worst case. Also, the result for the 384-keV peak is not consistent with the general results in this section.

TABLE II
DIFFERENCES IN SIMULATED AND REAL HPGE DETECTOR EFFICIENCY LOWER ENERGY

Isotope	Region	Energy	Efficiency Difference (Simulated - Measured)
137Cs	Photopeak	32 keV	-41.7 %
	Photopeak	36 keV	-30.3 %
133Ba	Photopeak	31 keV	-45.0 %
	Photopeak	35 keV	-28.8 %
	Photopeak	53 keV	-4.3 %
	Photopeak	80 keV	3.4 %
	Photopeak	276 keV	9.5 %
	Photopeak	302 keV	9.9 %
	Photopeak	356 keV	7.6 %
	Photopeak	384 keV	-4.0 %
	Total	40-1000 keV	-1.2 %

D. Conclusions of the Verification

For the energy regions of interest to this work, qualitative and quantitative comparisons of real and simulated spectra show that the simulation tool is able to reproduce the spectroscopic behavior of an HPGe detector operating in the presented geometry. Total efficiency estimates are in good agreement with the experimental values, while gamma photopeak efficiencies agree to within 4–10% depending on the photopeak energy. Unacceptable discrepancies have been found for X-ray photopeaks under 40 keV, so the code is considered to be valid for our purposes above this energy.

IV. CONSIDERATIONS FOR THE SIMULATION OF CZT DETECTORS

A. Detector Anode Bias Polarity

The detector configuration always has one anode, denoted as A1, and the peripheral electrode (guard ring) connected to ground. The other anode, A2, can be biased at either positive or negative potential and selects the collecting anode. This polarity selection for A2 affects detector properties such as resolution and efficiency. The central region of the detector is insensitive to the A2 polarity due to the anode grid symmetry in this area, but the collection of the charge generated in the volume underneath the peripheral electrode and in the gaps between this electrode and the central region are affected by this polarity. Let us denote by G1 and G2 the gap areas between the peripheral electrode and A1 and between the peripheral electrode and A2, respectively (see viewgraph in Fig. 3). Significant differences in the collection of the charge generated outside of the central region may occur.

B. Effect of A2 Anode Polarity on the Detector Efficiency and Resolution

Biasing A2 negatively would lead to regions where the electrons are not transported efficiently when the differential readout method (total pulse amplitude is computed from a weighted difference between A1 and A2 pulse amplitudes [7]) is used. Volumes underneath the peripheral electrode and G2 will produce pulses with negligible amplitude. On the

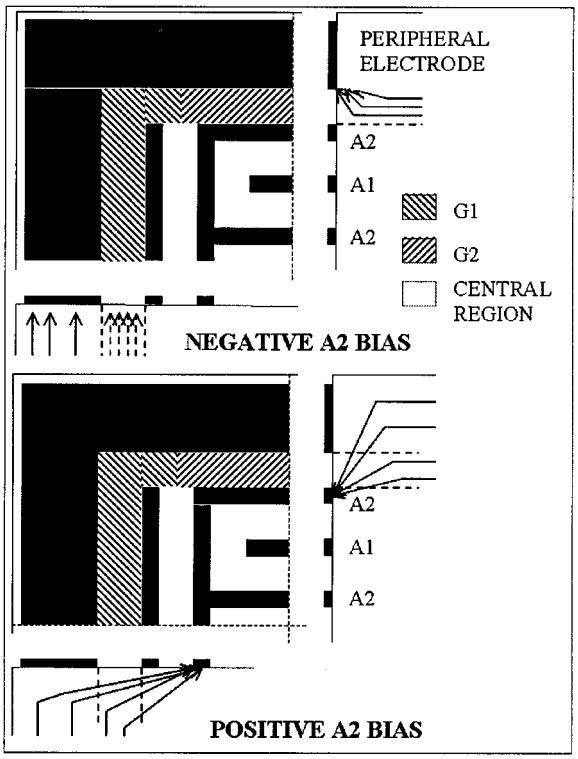

Fig. 3. Schematic representation of one of the detector anode surface corners. Peripheral electrode and collecting and noncollecting anode are represented. Arrows show charge-collection trends in the two-anode bias configuration.

other hand, pulses with significant amplitude can be induced from photons interacting in region G1. Most of the photons interacting in this region will not contribute to the photopeak.

When A2 is biased positively, pulses produced from region G2 are correctly formed using the differential readout method. This region of the detector will contribute to the spectrum, although with some spectral degradation due to the electrode profile in this region. Charges produced in region G1 will drift to the nearest A2 anode strip. Their path to A2 is much larger than the corresponding path in the central region and proceeds through a region with a weak electric field. These two factors increase the probability of electron trapping. The region underneath the peripheral electrode can also be sensitive in this case, but the charge-trapping probability due to the longer drift length is even larger. Thus, A2 positive biasing will lead to a higher detector efficiency. On the other hand, more spectral degradation can be expected using positive biasing, since a photon interacting in the detector periphery suffers from a nonideal drift to the collecting anode.

The actual areas of the G1, G2, and peripheral electrodes can be estimated from the detector dimensions. Significant differences (∼25–30%) in the detector efficiency can be expected depending on the applied anode bias. When the A2 anode is biased negatively, anode A1 collects ∼70% of the total interactions in the crystal, and the peripheral electrode should collect ∼25%. Any photons interacting in the G1 region are unseen. When A2 has a positive bias, all the charge should drift to the collecting anode.

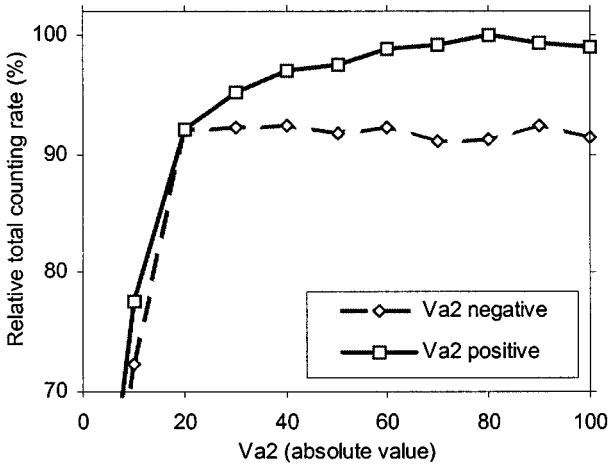

Fig. 4. Relative total counting rates obtained with detector I9-01 for different (positive and negative) A2 anode biasing values. Source: ^{137}Cs. (Lines to guide the eye.)

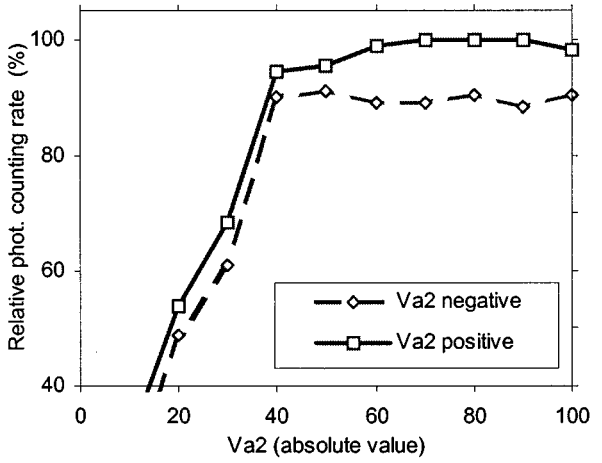

Fig. 5. Relative photopeak (662 keV) counting rates obtained with detector I9-01 for different (positive and negative) A2 anode biasing values. Source: ^{137}Cs. (Lines to guide the eye.)

C. Experimental Confirmation

Differences in the detector efficiency have been experimentally observed. Figs. 4 and 5 present relative total and photopeak efficiencies measured with detector I9-01, covering a wide range of positive and negative A2 anode biasing values but using the same geometric conditions. A ^{137}Cs source was used for these measurements. Each detector bias configuration was stable for a period of 15 min, and data were reproducible.

With A2 positively biased, both the total and absolute efficiency reach a maximum value near +80 V. A2 negatively biased led to more stable values over the complete range of useful bias values. Comparing the best measurement when A2 is positively biased to the average value when negatively biased, the total and photopeak absolute efficiencies differ by 8% and 10%. This is qualitatively consistent with the discussion above, although larger differences were expected.

Better spectroscopic resolution was achieved with negative A2 anode biasing for all bias values presented in Fig. 5 (∼2.5% FWHM in the best case). ∼0.5% FWHM poorer resolution was found if the positive anode bias was used. Photopeaks using an

A2 positive bias showed a less regular shape, presenting shoulders or side lobes.

To obtain information about the signal generated at the peripheral electrode, the corresponding pin in the detector was connected to a charge-sensitive preamplifier. The external bias input remained grounded. The output signal was filtered using a shaping amplifier, and spectra were acquired. The data obtained under different bias polarities for A2 showed that while a positive anode bias does not ensure that all the charges drift to the collecting anode, the number of pulses that drift to the peripheral electrode ($\sim$3%) can be considered as minor. Furthermore, the 12% fraction of events collected by the peripheral electrode in negative anode bias configuration is lower than expected. From geometry, the peripheral electrode could act as the collecting electrode for $\sim$25–30% of the pulses.

V. Simulation of the CZT Detectors

A. Detector Efficiency Simulation

The coplanar CZT detectors were mounted on a poly vinyl chloride (PVC) support attached to the aluminum box that houses the front-end electronics and the subtraction circuit. Detectors were carefully positioned, the source was located outside the box in front of the detector, and a hole in the box minimized the material along the detector–source axis. The hollow area was covered by a 0.2-mm thin copper foil to ensure electromagnetic shielding without inducing radiation scattering. Only the substrate front layer of the detector presented any significant matter between the source and the CZT crystal. The distance from the source to the detector center in the external surface of its support was fixed within 0.2 mm. The point source was located normal to the cathode surface. Layers of lead surrounding the housing box made the background contribution negligible compared with the counting rate with sources in place. The biases were -1700 V for the cathode and -80 V for the noncollecting anode (0 V for collecting and peripheral anodes).

The experimental setup described in previous paragraph were simulated. Mechanical and electrical components in the setup have been modeled with different degrees of fidelity, depending on their potential influence to the radiation scattering and absorption. The lead shielding was included in the model. From the arguments above, the expected sensitive volume in this detector configuration is just the central region. Only the central section of 1.2865×1.2865 cm area was modeled as active.

B. Detector I9-04

1) Higher Energy: Simulated and real spectra were acquired, and some results are presented in Figs. 6 and 7 for ^{137}Cs. Quantitative differences between real and simulated absolute efficiency are presented in Table III for different regions of the spectra. In some cases, photopeak limits in the simulated and real spectra had different end points, according to the peak search criteria.

Simulation and measurement results differ at low energies. As expected from our experiments with the HPGe detector, experimental detector efficiency is not correctly estimated for X-ray photopeaks, and a significant accumulation can be observed in the real spectrum under 120 keV. Pulses resulting from poor charge transport are responsible for these low-energy counts [3].

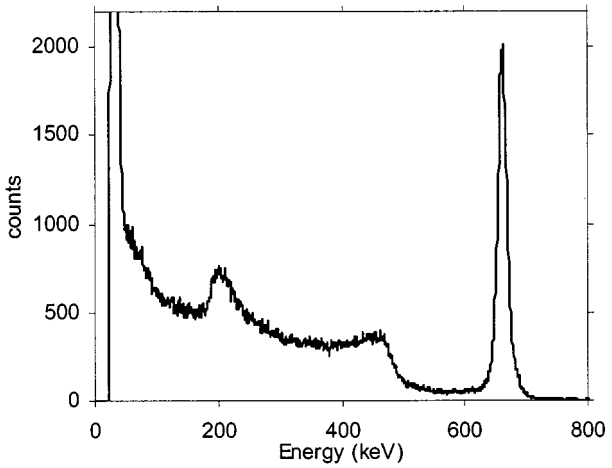

Fig. 6. Real spectrum acquired with I9-04 detector and the ^{137}Cs source. Acquisition time corresponds to 100-s live time. Detector–source distance was 1.86 cm.

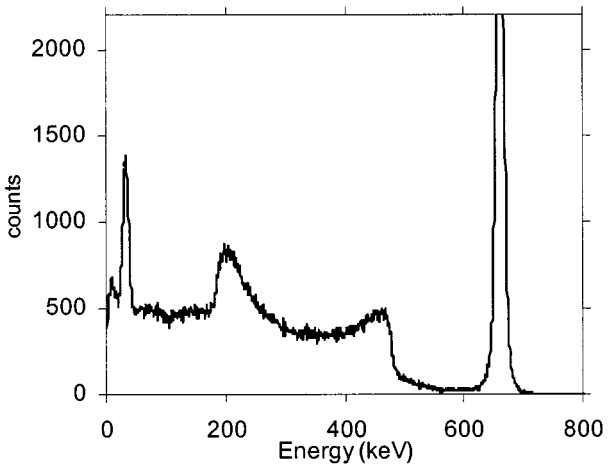

Fig. 7. Simulation of the spectroscopic response of the I9-04 detector ^{137}Cs considering the experimental situation used for acquiring the spectrum in Fig. 6.

The total detected counts in the real and simulated spectra agree to within 5%, only slightly larger than the source activity uncertainty. This fact supports the premise that the central region is the only sensitive part of the detector. A portion of the counts below 60 keV, assumed to be produced by X-rays, may belong to the low energy accumulation. However, the Compton area is underestimated in the simulation. Since there is a reasonable agreement in the total counts, this suggests that there are more pulses than expected in the Compton region of the real spectrum, also reflected in the significant disagreement in the photopeak efficiency. As shown in Table III, $\sim$35% of the expected pulses in the photopeak are missing in the real spectrum. Charges that do not follow the ideal drift profiles alter the spectrum shape, shifting counts to lower channels.

The low energy accumulation was also observed using digital techniques when the A2 anode was biased to $+80$ V. Unexpected pulse-height distributions and proportions were similar

TABLE III
DIFFERENCES IN SIMULATED AND REAL I9–04 DETECTOR EFFICIENCY

Isotope	Region	Energy	Efficiency Differences (Simulated - Measured)
137Cs	Photopeak	32-36 keV	-57.9%
	Compton	60-620 keV	-1.5 %
	Photopeak	662 keV	34.8 %
	Total	60-715 keV	4.7%
	Peak (662 keV) to Total ratio:		28.7 %
60Co	Compton	40 – 1137 keV	-3.6%
	Photopeak	1173 keV	36.1%
	Photopeak	1333 keV	38.1%
	Total	24-1367 keV	-4.4 %
	Total	40-1367 keV	-0.8 %
	Peak (1173 keV) to Total ratio:		37.2 %
	Peak (1333 keV) to Total ratio:		39.2 %
133Ba	Photopeak	31-35 keV	-59.6 %
	Photopeak	82 keV	37.9 %
	Photopeak	302 keV	37.3 %
	Photopeak	356 keV	37.7 %
	Total	47-410 keV	13.3 %
	Total	60-410 keV	16.4 %

to those obtained for negative bias. This result supports the idea that these distributions are independent of peripheral region effects and are generated in the detector central region.

The results obtained for ^{60}Co show characteristics similar to those from the study using ^{137}Cs. In this case, there is no contribution due to X-rays, so it was decided to set a lower energy limit of 24 keV. There was still good agreement between expected and real total efficiency, but the measured absolute photopeak efficiency was again lower than predicted.

2) Lower Energy: Results obtained using ^{133}Ba are presented in Table III. Absolute peak efficiency is used except for the 82- and 302-keV lines, which use net efficiency since a net area seems to be more realistic. Differences will go down to 31.5% for the 82-keV peak in Table III if the absolute number of counts were used. Only photopeaks with consistent statistics have been taken into account. Photopeaks of 276 and 384 keV are greatly affected by the major contribution of other lines in their respective multiplets.

The total efficiency estimate fails in this case, since the difference between expected and real values ∼15%, which is larger than the acceptable error. This difference decreases for lower energy thresholds. Unfortunately, it is not possible to consider threshold values under 47 keV due to the serious discrepancy in the 31–35 keV peak estimate.

3) Results of the Study With I9-04 Detector: Our results studying the efficiency of the CZT I9-04 coplanar grid detector are summarized as follows.

1) Comparison of results obtained from experimental and simulated spectra shows a general agreement for the total counting rate in the energy range of interest. The negative anode bias configuration was predicted only to have the central part of the detector be sensitive. The result confirmed that the efficiency in the anode grid central region is as expected. Worse agreement was achieved for total efficiency for energies below 400 keV.
2) A very large fraction of the pulses in the spectrum are spread over energies lower than the corresponding deposited energy. This fraction is ∼35% for the photopeaks examined (82, 302, 356, 662, 1173, and 1333 keV). We conclude that the charge drift/collection process is less than ideal in the detector central region.

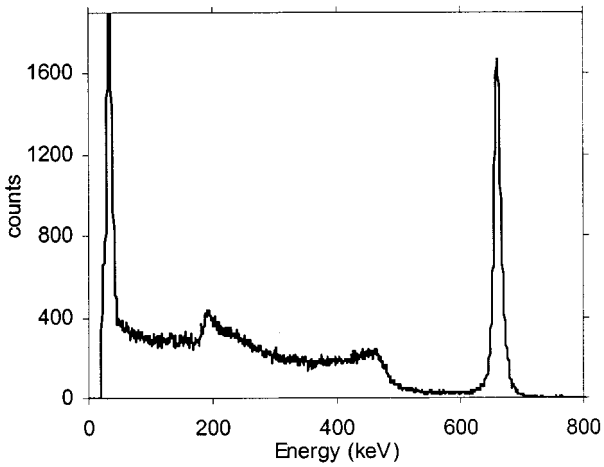

Fig. 8. Real spectrum acquired with I9-01 detector and ^{137}Cs source. Acquisition time corresponds to 100-s live time. Detector–source distance was 2.95 cm.

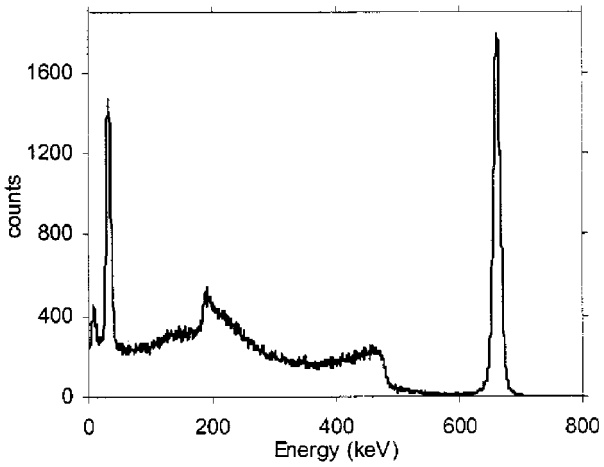

Fig. 9. Simulation of the spectroscopic response of the I9-01 detector for ^{137}Cs considering the experimental situation used for acquiring the spectrum in Fig. 8.

C. Detector I9-01

Examples of comparable experimental and simulated spectra are presented in Figs. 8 and 9 for ^{137}Cs. Quantitative differences between simulated and real estimations for total, Compton, and photopeak counting efficiencies are listed in Table IV. These data show an acceptable general agreement between real and simulated spectra. The most remarkable result is the general agreement not only in the total efficiency but also in the photopeak efficiency. This agreement is not perfect, but evident in the most important lines.

TABLE IV
DIFFERENCES IN SIMULATED AND REAL I9-01 DETECTOR EFFICIENCY

Isotope	Region	Energy	Efficiency Differences (Simulated - Measured)
137Cs	Photopeak	32-36 keV	-30.6%
	Compton	60-620 keV	-0.7%
	Photopeak	662 keV	-0.5%
	Total counts	60-715 keV	-0.7%
	Total counts	46-715 keV	-1.9%
	Peak (662 keV) to Total ratio:		-0.4 %
60Co	Compton	40-1149 keV	-0.7%
	Photopeak	1173 keV	-1.4%
	Photopeak	1333 keV	0.1%
	Total counts	40-1390 keV	-1.8%
	Total counts	24-1390 keV	-3.3%
	Peak (1173 keV) to Total ratio:		0.7 %
	Peak (1333 keV) to Total ratio:		0.7 %
133Ba	Photopeak	31-35 keV	-27.7%
	Photopeak	82 keV	-0.7%
	Photopeak	276 keV	-5.9%
	Photopeak	302 keV	-0.3%
	Photopeak	356 keV	1.5%
	Photopeak	384 keV	-5.0%
	Total	70-410 keV	-2.2 %
	Total	48-410 keV	-5.1 %

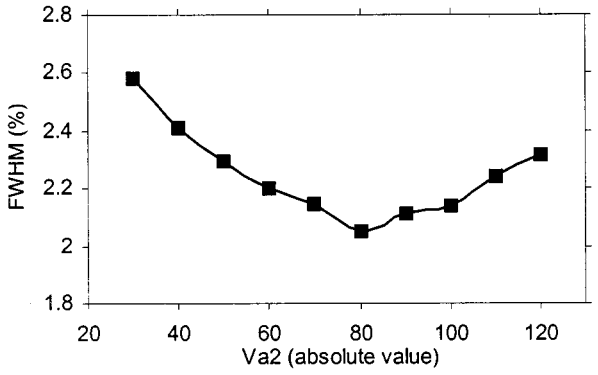

Fig. 10. Resolution of the I9-01 detector for different negative values of A2 bias and cathode bias set to −1700 V. Anode A1 and peripheral anode were grounded.

1) Results for Photopeak Efficiency: The fact that an acceptable agreement was reached between the experimental and theoretical efficiencies in this detector has important consequences. First, the electrode design used in the detector (generation II [4]) is efficient. Data in Figs. 5 and 10 reinforce this conclusion. In the latter figure, the measured resolution of the detector is presented for different negative anode bias values. Experimental data were obtained with the geometry and setup modeled in the simulation. Once the anode bias reaches ∼40 V, the photopeak efficiency is constant, and an acceptable energy resolution is obtained.

2) Possible Sources of Uncertainty in the Calculations: The uncertainty in the simulated results due to uncertainty in the detector–source positioning was estimated by changing the distance from the detector to the source. For a change of 0.05 cm, the maximum experimental uncertainty in this distance, a change of ∼3% both in the photopeak and the total efficiency was determined.

Other important sources of uncertainty include the source activity and the calculation of the photopeak area. The selection of the limits of the photopeak is in some cases ambiguous. This uncertainty makes the uncertainty associated with the photopeak area ∼5%. A precise estimate of this value is difficult since it depends on the particular spectrum profile in the peak region. For instance, 276-keV (^{133}Ba) and 302-keV (^{133}Ba) photopeaks are affected by larger uncertainties in their counting estimates than 662-keV (^{137}Cs), 1333-keV (^{60}Co) or 82-keV (^{133}Ba) photopeaks. The 1173-keV (^{60}Co) line is especially problematic due to its position between 1333-keV peak and the Compton edge. The limits for this peak must be examined carefully for each particular spectrum.

Statistical errors associated with the simulation have been estimated by running the code repeatedly for the same input values. Standard deviations for the total efficiency values are below 0.25% for ^{137}Cs and ^{60}Co, and are smaller for ^{133}Ba (0.12%). Standard deviations found for photopeak efficiency estimates are ∼0.3% for ^{137}Cs and ^{137}Ba photopeaks, except for 276 and 384 keV, in which larger values were found (∼0.85%). ^{60}Co photopeaks presented the largest uncertainty values: 0.93% and 1.37% for 1173- and 1333-keV photopeaks, respectively.

VI. MODELING NONIDEAL CHARGE COLLECTION

A. Simulation of an Inefficient Anode Design

Results obtained for detector I9-01 show that the electrode design permits efficient collection within the detector's central region. We shall assume that both detectors had the same surface treatment and electrode deposition processes. Thus, the most probable cause of the photopeak efficiency loss in detector I9-04, common in many CZT crystals, is a larger proportion of defects in the bulk material.

Another possible cause for this efficiency loss we now consider are regions in detector I9-04 in which the electric field profile is not high enough to correctly bend the carriers to the collecting anode. These regions should be located underneath the noncollecting anode strip and could be caused by an imperfect electrode deposition process. In this case, those interactions beneath one of the noncollecting strips would generate carriers that do not drift to the collecting anode. As a consequence, the generated pulse from the anodes would be smaller. We consider two collection models here.

1) Model CM1: charge produced in some regions under the noncollecting strips is drifted to this anode.
2) Model CM2: charge does not reach the anode surface due to weak electric field intensity in some region under the noncollecting strips.

The widths of the anode and the gap strips in these detectors are 0.0152 and 0.0355 cm, respectively. The lateral width of the charge cloud just due to the diffusion of the electrons produced by the radiation in a single point of these detectors is of this order of magnitude [8]. Thus, electron diffusion must be taken into account.

The code has been adapted for modeling a region under the noncollecting anode strips in which charge is not collected by the collecting anode. In this new version, each portion of the charge produced in a single point of the detector is studied separately. The charge is drifted from the interaction point to the plane 1 mm from the anode surface and follows the electric field lines. This trajectory is perpendicular to the anode surface since the electric field can be considered constant in this region of the detector. During this drift, charge is diffused according to the basic distribution described in [8]. Once cloud i reaches the plane 1 mm from the anode, the portion P_i of the cloud located directly under the central region of the noncollecting strips is computed. The width of this region is given by f_c times the noncollecting strip width, where f_c can be varied from 0.0 (all the charge correctly collected) to 1.0, the total strip width.

The amplitude of the pulses is generated from the two collection models.

1) In Model CM1, the amplitude A of the pulse is generated by

$$\begin{aligned} A =& C \cdot \sum_{i=1}^{n} ((1-P_i)Q_i - P_iQ_i) \\ =& C \cdot \sum_{i=1}^{n} (1-2P_i)Q_i \end{aligned} \tag{1}$$

where C is a constant and Q_i is the number of electrons generated by the radiation at the point r_i $(i = 1, \ldots, n)$. The first term in the sum corresponds to the portion of the charge correctly collected. The second part is the portion collected by the noncollecting anode. This portion has a negative net contribution, since the differential readout spectroscopic method is used.

2) For Model CM2, the pulse amplitude is

$$A = C \cdot \sum_{i=1}^{n} (1-P_i)Q_i. \tag{2}$$

In this case, the charge that is not collected contributes in the same way to both the collecting and noncollecting pulses, so its net contribution is zero.

B. Results of Charge Collection Modeling for Detector I9-04

Different widths for the "dead" region underneath the noncollecting anode strips have been considered by varying $f_c = 0.05$ to 1.0. Figs. 11 and 12 present graphic results for some representative cases of f_c using the two collection models.

For model CM1, a ∼30% reduction of the photopeak counts is achieved for $f_c = 0.25$, while the total number of counts (60–710 keV) remained almost constant. Similar results are found considering model CM2 for $f_c = 0.50$ (∼31 and ∼2% of photopeak and total efficiency reduction, respectively.) These charge collection models can explain the photopeak efficiency loss of detector I9-04. But neither model predicts the low energy accumulations of the magnitude observed for detector I9-04. However, the modeled photopeaks do show low-energy tailing not seen in the measured spectra.

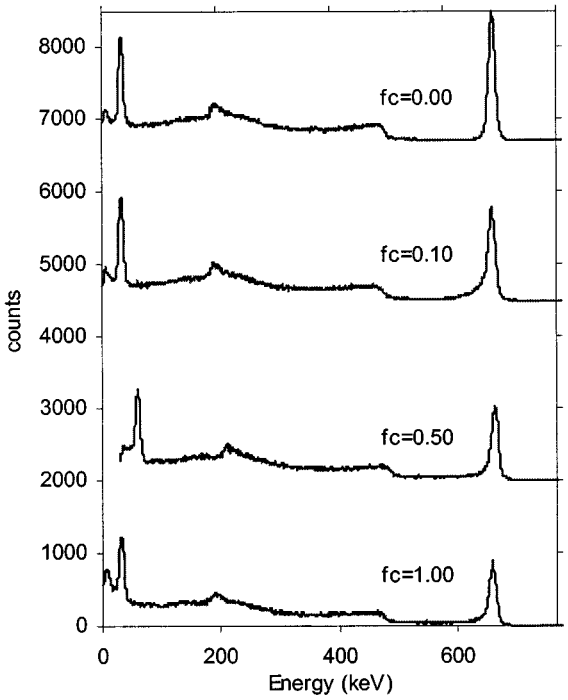

Fig. 11. Spectra obtained using collection model CM1 for f_c ranging from 0.05 to 1.0 (f_c being the relative width of the layer under noncollecting anode strips in which generated charge is not collected by the collecting anode).

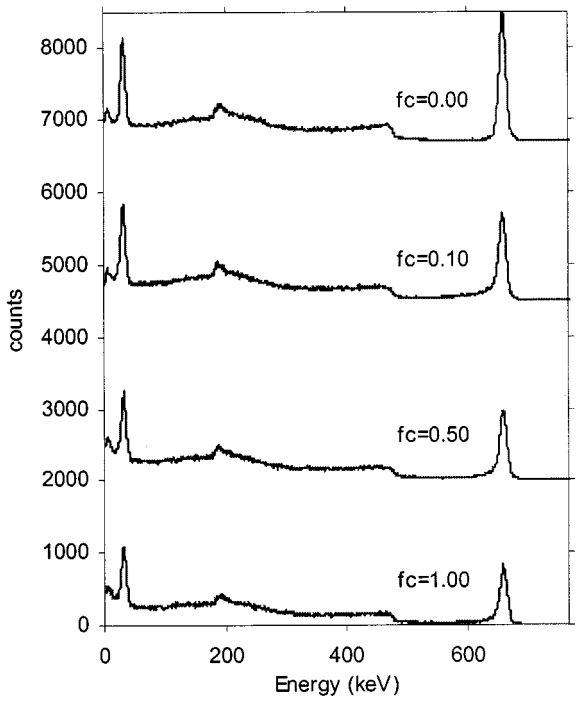

Fig. 12. Spectra obtained using collection model CM2 for f_c ranging from 0.05 to 1.0 (f_c being the relative width of the layer under noncollecting anode strips in which generated charge is not collected by the collecting anode).

The presented charge drift models are not sufficient to attribute the behavior of detector I9-04 to charge transport inefficiencies from the detector electrode design nor due to factors related to the electrode deposition process. Having ruled out this possibility, we can say that the probable cause of the detector

degradation is the presence of regions with an accumulation of defects within the detector.

VII. Conclusion

The electrode design of detector I9-01 is efficient. There is no need for designs with a larger number of strips per anode and narrower gaps. Further work is needed to understand the role of energy resolution in the anode plane direction perpendicular to anode strips. If no large differences were found between spectroscopic performances under the gaps and collecting and noncollecting strips, this would imply that the only major cause of resolution loss is related to the existing differences in the collecting and noncollecting anode weighting potentials. Obviously, this result also implies that the material used in the detector is of sufficient quality.

From results obtained with detector I9-04, nearly one-third of its volume is affected by defects that limit charge transport and collection, affecting detector spectroscopic performance. Further studies on the detector solid-state physics and real electric field distribution might be carried out for a full characterization of the detector. This continuation, which represents a significant amount of work, has been started in our laboratory and will be the subject of a future publication.

The two detectors perform differently. The I9-04 unit behaves like a low-quality detector, whereas I9-01 seems almost ideal. Yet our experience in the laboratory leads to a different conclusion. In spite of its lower photopeak efficiency, I9-04 demonstrated an excellent stability in long-term tests [3]. On some occasions, the experimental performance for I9-01 could not be sustained longer than seven days. After this period, the detector showed an increase in the leakage current, and discharge pulses were observed. Serious low-frequency drifts in the baseline of anode and cathode lines were also observed in these states. Thus, for some applications, detector I9-04 may actually be preferable. Studying a great population of similar units is desirable to identify trends in the performance of these kind of detectors. Unfortunately, the lack of timely availability of such detectors limits these kinds of study.

Acknowledgment

The authors would like to thank H. Downey for his validation of the simulation tool with the Ge detector and his help in the Ge spectra acquisition and P. Simpson for his aid in the experimental spectrum format conversion. Thanks are also given to CIEMAT's D. Francia, who performed most of the graphic editing of figures. The authors also acknowledge the computing support given by A. Roldan and J. Calonge, both from CIEMAT, who efficiently managed the installation and updating of libraries and the operating system.

References

[1] P. N. Luke, "Unipolar charge sensing with coplanar electrodes. Application to semiconductor devices," *IEEE Trans. Nucl. Sci.*, vol. 42, pp. 207–213, Aug. 1995.

[2] Z. He, G. K. Knoll, D. K. Wehe, and J. Miyamoto, "Position-sensitive single carrier CdZnTe detectors," *Nucl. Instrum. Methods*, vol. A388, pp. 180–185, 1997.

[3] J. M. Perez, Z. He, and D. K. Wehe, "Stability and characteristics of large CZT coplanar electrode detectors," *IEEE Trans. Nucl. Sci.*, vol. 48, pp. 272–277, June 2001.

[4] Z. He, G. K. Knoll, D. K. Wehe, and J. F. Du., "Coplanar grid patterns and their effect on energy resolution of CdZnTe detectors," *Nucl. Instrum. Methods*, vol. A411, pp. 107–113, 1998.

[5] CERN Program Library Office. GEANT 3.21 detector description and simulation tool. [Online]. Available: http://www.cernlib@cern.ch

[6] The Geant4 collaboration. (2002, Mar.) Geant4. [Online]. Available: http://wwwinfo.cern.ch/asd/geant4/geant4.html

[7] Z. He, G. K. Knoll, D. K. Wehe, R. Rojeski, C. H. Mastrangelo, M. Hamming, C. Barret, and A. Uritani, "1-D position sensitive single carrier semiconductor detectors," *Nucl. Instrum. Methods*, vol. A380, pp. 228–231, 1996.

[8] Y. F. Du, Z. He, W. Li, G. F. Knoll, and D. K. Wehe, "Monte Carlo investigation of the charge sharing effects in 3-D position sensitive CdZnTe gamma ray detectors," *IEEE Trans. Nucl. Sci.*, vol. 46, pp. 844–847, Aug. 1999.